An Integrated Approach to Estimate Instantaneous Near-Surface Air Temperature and Sensible Heat Flux Fields during the SEMAPHORE Experiment

DENIS BOURRAS

NASA Jet Propulsion Laboratory, California Institute of Technology, Pasadena, California

LAURENCE EYMARD

Centre d'Etude des Environnements Terrestre et Planétaires, Velizy-Villacoublay, France

W. TIMOTHY LIU

NASA Jet Propulsion Laboratory, California Institute of Technology, Pasadena, California

HÉLÈNE DUPUIS

Université Bordeaux I, Talence, France

(Manuscript received 4 December 2000, in final form 10 September 2001)

ABSTRACT

A new technique was developed to retrieve near-surface instantaneous air temperatures and turbulent sensible heat fluxes using satellite data during the Structure des Echanges Mer–Atmosphere, Proprietes des Heterogeneites Oceaniques: Recherche Experimentale (SEMAPHORE) experiment, which was conducted in 1993 under mainly anticyclonic conditions. The method is based on a regional, horizontal atmospheric temperature advection model whose inputs are wind vectors, sea surface temperature fields, air temperatures around the region under study, and several constants derived from in situ measurements. The intrinsic rms error of the method is 0.7°C in terms of air temperature and 9 W m^{-2} for the fluxes, both at 0.16° × 0.16° and 1.125° × 1.125° resolution. The retrieved air temperature and flux horizontal structures are in good agreement with fields from two operational general circulation models. The application to SEMAPHORE data involves the *First European Remote Sensing Satellite* (*ERS-1*) wind fields, Advanced Very High Resolution Radiometer (AVHRR) SST fields, and European Centre for Medium-Range Weather Forecasts (ECMWF) air temperature boundary conditions. The rms errors obtained by comparing the estimations with research vessel measurements are 0.3°C and 5 W m^{-2}.

1. Introduction

Turbulent heat flux fields at the air–sea interface are necessary to study the upper-ocean heat budget or to force ocean general circulation models (GCMs). These flux fields may be obtained mainly from atmospheric GCMs or satellite data.

GCMs produce a physical and dynamical interpolation in space and time between in situ measurements. However, there are often large uncertainties in the analyses because observations are sparse at a global scale and the boundary layer models implemented in GCMs are not accurate. The analyzed horizontal atmospheric temperature and turbulent flux structures are consequently often mislocated. Satellite data are increasingly used to retrieve the fluxes because they are observations and have a high temporal and spatial sampling. Although methods have been developed to derive the latent heat flux from satellite data (Liu and Niiler 1984; Bourras et al. 2001), the sensible heat flux H_s depends in part on the near-surface air temperature, which is a difficult parameter to retrieve from space. At a 1-month scale, Jones et al. (1999) find a statistical relationship between individual surface air temperature (T_A) measurements and columnar water vapors and wind speeds derived from satellite observations. The retrieval error of their method is 0.72° ± 0.38°C. Clayson and Curry (1996) propose to derive air temperatures from satellite-derived humidities q_A and cloud-top temperature measurements. The root-mean-square (rms) error is 0.77°C. However, their method loses accuracy as relative humidity increases and needs very accurate sea surface temperatures (SST) as inputs. Konda and Imasato (1996) proposed a method based on a Bowen ratio that uses

Corresponding author address: Denis Bourras, NASA Jet Propulsion Laboratory, MS300-323, 4800 Oak Grove Dr., Pasadena, CA 91109.
E-mail: bourras@pacific.jpl.nasa.gov

satellite-derived winds, SSTs, and q_A as inputs. The retrieval errors at 1-month scale are $-0.3° \pm 3.1$°C for T_A and 10.0 $\pm$ 37.6 W m^{-2} for H_s. Another approach validated—qualitatively—at this timescale is the global advective atmospheric mixed-layer model proposed by Seager et al. (1995). The inputs are only global SSTs and surface wind fields.

In this paper, we propose a computationally fast physical method to obtain high-spatial-resolution (0.3° × 0.3°) instantaneous T_A and H_s fields. The method is based on a horizontal temperature advection model (ADMOD), which may be considered to be a simpler version of Seager's model. The method presented here is useful in the context of field experiments because it works on mesoscale regions (1000 km × 1000 km) and uses as inputs a combination of satellite data, operational GCM analyses, and in situ measurements. The input variables are SST, horizontal wind vector fields, and T_A around the region under study. In this paper, ADMOD is applied to European Remote Sensing Satellite (*ERS-1*) wind vectors, SST maps from the National Oceanic and Atmospheric Administration Advanced Very High Resolution Radiometer (AVHRR), and boundary T_A from operational analyses. The method is validated using research vessel (R/V) in situ measurements and GCM fields from the Structure des Echanges Mer–Atmosphere, Proprietes des Heterogeneites Oceaniques: Recherche Experimentale (SEMAPHORE) experiment, which was conducted in autumn of 1993 near the Azores Islands under mainly anticyclonic meteorological conditions (Eymard et al. 1996).

The paper is organized as follows: the method is described in the next section and the datasets are presented in section 3. Then, ADMOD physics are validated on GCM data, which allows a comparison on a large amount of situations, and a sensitivity study is done (section 4). Last, T_A and H_s are derived using satellite data during SEMAPHORE, they are compared with R/V measurements and GCM fields (section 5), and conclusions follow.

2. Method

Under the assumptions of nonviscous steady flow and horizontal homogeneity of turbulence and mean flow, the mean potential temperature conservation equation at altitude z_A may be written as

$$\mathbf{u} \cdot \nabla T_A = -\frac{\partial \overline{w'\theta'}}{\partial z} - \delta_R, \tag{1}$$

where $\mathbf{u}$ is the horizontal wind vector, T_A is now the mean potential temperature, $\overline{w'\theta'}$ is the turbulent sensible heat flux, and δ_R is the radiation flux divergence term. The turbulent flux may be considered as decreasing linearly with height until the top of the mixed layer at which it vanishes (Kwon et al. 1998), so that the flux term in (1) becomes

$$\frac{\partial \overline{w'\theta'}}{\partial z} = -\frac{\alpha}{h}\overline{w'\theta'}_{\text{surf}}, \tag{2}$$

where α is a dimensionless coefficient, h is the mixed-layer height, and $\overline{w'\theta'}_{\text{surf}}$ is the turbulent flux in the constant-flux surface boundary layer. The flux is obtained from an iterative bulk algorithm denoted as f (Bourras 2000), based on the Dupuis et al. (1997) parameterization of the bulk coefficients. The inputs of this algorithm are $\mathbf{u}$, SST, T_A, the specific humidity β_{q_A}, and the sea level pressure γ_{p_S}. The eventual expression of the model is

$$\mathbf{u} \cdot \nabla T_A = \alpha h^{-1} f(\mathbf{u}, \text{SST}, T_A, \beta_{q_A}, \gamma_{p_S}) - \delta_R. \tag{3}$$

The unknown is T_A, and the input variables are $\mathbf{u}$ and SST. Parameters α, h, β_{q_A}, γ_{p_S}, and δ_R are assumed to be constant at the scale of the experiment. All of the constant coefficients are derived from in situ observations (section 3a) except δ_R, which is adjusted to GCM data (section 4a). The technique used to invert ADMOD numerically is described in appendix A.

3. Datasets

The data used were collected during the intensive observation period (IOP) of the SEMAPHORE experiment from 15 October to 15 November 1993 and covering 30°–38°N and 20°–28°W. The meteorological conditions were mainly anticyclonic during the campaign. The mean pressure at surface level was 1020 hPa. Only one active low pressure (1000 hPa) center crossed the SEMAPHORE area between 30 October and 1 November. According to R/V measurements, the mean values and rms deviations of scalar wind speed, T_A, and SST over the whole IOP are 7 $\pm$ 3.1 m s^{-1}, 20° $\pm$ 1.9°C, and 22° $\pm$ 1.3°C, respectively (Eymard et al. 1996).

Three types of data are described herein: ADMOD input data, ADMOD validation data, and an additional test dataset. ADMOD input data gather satellite $\mathbf{u}$ and SST fields, GCM data for T_A at the boundaries, aircraft measurements (α, h), and R/V observations (β_{q_A} and γ_{p_S}). Validation data are T_A and H_s from an R/V and two GCMs. The test data contain GCM fields only and are used separately from the other datasets to set δ_R and to check the intrinsic error of ADMOD.

a. ADMOD input data

In this section, the fields used as ADMOD inputs are described ($\mathbf{u}$, SST, and boundary T_A), the collocation method between the different fields is explained, and the coefficients z_A, α, h, β_{q_A}, and γ_{p_S} are set.

ADMOD input wind fields are *ERS-1* wind vectors at 0.3° × 0.3° resolution provided by Institut Francais de Recherche pour l'Exploitation de la Mer (IFREMER). The rms accuracy of these scatterometer fields is 1 m s^{-1} (Bourassa et al. 1997). High-resolution (0.09° × 0.09°) 8-day-averaged AVHRR SST fields were pro-

TABLE 1. List of the ECMWF, ARPEGE, and *ERS-1* dates and times.

Date	ECMWF/ARPEGE time (UTC)	*ERS-1* swath time (UTC)
10 Oct 1993	1200	1202
13 Oct 1993	1200	1208
19 Oct 1993	0000	0004
1 Nov 1993	1200	1211
4 Nov 1993	1200	1216
7 Nov 1993	0000	0006

vided by the Jet Propulsion Laboratory (JPL) Physical Oceanography Distributed Active Archive Center (PODAAC). The accuracy of the retrieval algorithm is 0.02° ± 0.5°C (Kilpatrick et al. 2001). Although these AVHRR SSTs are not instantaneous observations, they are used as ADMOD inputs to retrieve instantaneous T_A and H_s. The reason is that the SST varies weakly over short timescales, except in case of strong meteorological events. One strong event occurred during the IOP: the depression that crossed the SEMAPHORE region by the end of October of 1993 (see above) resulted in a cooling of the SST by 0.5°C in 3 days (Caniaux and Planton 1998). The corresponding data are not used in this study. Because the rest of the IOP was characterized by a slow decrease of the SST by 0.2°C a week (Caniaux and Planton 1998), the use of 8-day-averaged SST fields to retrieve the instantaneous T_A and H_s is a reasonable choice. Boundary T_A come either from 1.125° × 1.125° resolution operational analyses from the European Centre for Medium-Range Weather Forecasts (ECMWF) or from 0.16° × 0.16° reanalyses of the Météo France (French meteorological office) Action de Recherche Petite Echelle Grande Echelle (ARPEGE) atmospheric GCM (Giordani et al. 1998). The use of boundary T_A from operational analyses is generally the only possible choice to apply ADMOD, because no high-resolution reanalyses are available. In the context of SEMAPHORE, the availability of both analyses and reanalyses provides an opportunity to test the sensitivity of ADMOD to boundary conditions.

The *ERS-1* swaths are available over the SEMAPHORE region around 0000 and 1200 UTC each day. Orbits are selected in order that the time difference among *ERS-1,* ARPEGE, and ECMWF fields is minimum. The final dataset contains six cases, the dates of which are listed in Table 1. The maximum time difference among ECMWF, ARPEGE, and *ERS-1* fields is 16 min. In the following, the term ''case'' stands for the SEMAPHORE region at a particular date and time. ARPEGE fields and AVHRR maps are interpolated linearly at the *ERS-1* resolution, and the same process is applied to the ECMWF fields to avoid unrealistic discontinuities near the boundaries in ADMOD-estimated fields.

Parameter z_A is set to 17 m, which corresponds to the altitude of the lower level of the two GCMs used in this paper and also to the height of the R/V instrumented mast. The value of α is 1.2, according to Kwon et al. (1998, their Fig. 11 and Eq. 5). However, α is set to 1 because it slightly improves the accuracy of ADMOD estimates. Note that an α of 1 remains consistent with Kwon et al. (1998) findings given the 20%–25% scatter in their data. The reader is advised that this selection of α applies to SEMAPHORE conditions only. In environments warmer than SEMAPHORE, α may be larger than 1 because of the increased evaporation. The first step to account for evaporation in ADMOD would be to replace (2) by a parameterization of the vertical profile of buoyancy flux (Tennekes 1973). Parameter h is derived from the profiles of turbulence characteristics of the mixed atmospheric boundary layer measured by two aircraft (Lambert and Durand 1999; Kwon et al. 1998). The h mean value deduced from Kwon results is 580 m and its standard deviation is ±100 m. Parameter β_{q_A} is set to 10 g kg^{-1}, and γ_{p_S} is set to 1020 hPa, which are mean values derived from IFREMER R/V *Le Suroît* observations.

b. Validation data

The validation consists in comparing ADMOD T_A and H_s estimates to reference data. The reference data, presented below, are in situ R/V observations and GCM fields and are referred to local validation data and mesoscale field validation data, respectively.

Local validation data are measurements performed onboard of *Le Suroît.* Observation times are selected within a 4-h interval centered on the time of the six cases of Table 1. Research vessel data are averaged over 1-h periods resulting in four points of comparison for each case. The data consist of H_s, T_A, **u**, and SST. The last two parameters are added to the validation data because they are helpful to analyze the retrieval error of ADMOD.

Validation fields are the ECMWF analyses and the ARPEGE reanalyses described in section 3a. The ECMWF analyses are used to assess the quality of ADMOD output fields with respect to operational products. On the other hand, ARPEGE reanalyses are considered to be high-quality reference fields because most of the SEMAPHORE observations—including *Le Suroît* SST, T_A, and **u**—have been assimilated in these reanalyses (Giordani et al. 1998). Note that ADMOD output fields are not completely independent from ECMWF (or ARPEGE) fields given that ADMOD uses ECMWF (or ARPEGE) boundary T_A as input.

c. Test data

The test data consist of 32 ECMWF operational analyses at 1.125° × 1.125° resolution and 32 ARPEGE reanalyses at 0.16° × 0.16° from 15 October to 15 November 1993 at 0600 UTC, and covering 30°–38°N and 20°–28°W. The parameters extracted for each analysis (reanalysis) are **u**, SST, T_A, and H_s. These GCM fields

TABLE 2. List of the ECMWF and ARPEGE fields that correspond to strong anticyclonic conditions. The last column indicates the level of divergence of the horizontal wind field.

Date	Time (UTC)	$\nabla \cdot \mathbf{u}$ (10^5 s^{-1})
2 Nov 1993	0600	4.7
4 Nov 1993	0600	4.5
13 Nov 1993	0600	3.9
14 Nov 1993	0600	5.6
15 Nov 1993	0600	4.4

are used to check ADMOD physics and to adjust the value of δ_R, as detailed in the next section.

4. Validation of the method

In this section, GCM fields are used to adjust the value of δ_R and to check the validity of ADMOD physics, that is, the validity of the assumptions made and the parameterizations chosen in section 2. With this aim in view, ADMOD is successively run using different values of δ_R and with wind vectors, SST fields, and boundary T_A from two GCMs as inputs. The ADMOD T_A and H_s obtained at each run are then compared with the original GCM T_A and H_s fields in terms of rms deviation and bias. The optimal value of δ_R is the value for which the rms deviation and the bias are the smallest. The deviations observed when δ_R is optimal give the intrinsic error of ADMOD. GCM data used in this section are the ECMWF analyses and the ARPEGE reanalyses of the test dataset (section 3c). The use of these two GCMs allows one to check the influence of spatial resolution on the quality of ADMOD estimates. Parameters α, h, β_{qA}, and γ_{p_S} are set to the values defined in section 3a.

a. ADMOD versus ECMWF

ADMOD is applied to **u**, SST, and boundary T_A from 32 ECMWF analyses (section 3c). Because the resolution of the ECMWF analyses is 1.125° × 1.125°, the SEMAPHORE area corresponds to 7 × 7 pixels, which is very small. The workable number of pixels is even smaller (6 × 6 pixels) because the use of upwind finite differences takes one pixel around the region under study. To avoid this problem, the ECMWF fields were interpolated linearly at the ARPEGE resolution before applying ADMOD. Then, the ADMOD estimates obtained were interpolated back at 1.125° × 1.125°.

Five out of the 32 cases are considered apart because they correspond to strong-divergence cases; they are listed in Table 2. On the remaining 27 low-divergence cases, δ_R is first set to 0°C day^{-1}. For this value of δ_R, the rms deviation between estimated ADMOD T_A and original ECMWF T_A is 0.69°C. The bias is 0.52°C, and the correlation coefficient 0.92. The positive bias indicates that the temperature estimates are too warm because of the lack of cooling by the radiation fluxes. The optimal δ_R found on the ECMWF analyses is 0.5°C day^{-1}. For this value of δ_R, the rms deviation between ECMWF and ADMOD T_A is 0.66°C, or 3.4% (Fig. 1a). The bias is 0.17°C, the correlation coefficient is 0.93, and the peak deviations are +3.2° and −2.3°C, respectively. These results point out that radiation fluxes mainly affect the retrievals as a bias. The rms would likely be reduced if δ_R was not constant, which would imply the use of a radiative transfer model to account for vertical humidity and temperature profiles, and cloud cover. In the following sections, δ_R is 0.5°C day^{-1}.

Twenty-four out of the 27 fields obtained from ADMOD fit very well the ECMWF fields. Indeed, in each of these 24 cases the correlation coefficient between ADMOD and ECMWF T_A fields is always greater than 0.8. In a minority of cases (3 out of 25) the correlation coefficient is lower than 0.3. In these last three cases, strong atmospheric fronts are present and a horizontal advection model is too simple to render the complicated relationship between thermal and wind structures. In terms of H_s, the correlation between ADMOD and ECMWF for all data is 0.86, the rms deviation is 8.6 W m^{-2}, and the bias is −4.6 W m^{-2} (Fig. 1b).

In the five anticyclonic cases, the rms deviation between ADMOD and ECMWF T_A fields is 1.06°C and the correlation coefficient is 0.73. This large deviation between ADMOD and ECMWF fields is related to the particular configuration of the streamlines. Indeed, in each of the five cases the anticyclone is so large that most of the boundary conditions are outflow conditions. The main inflow condition in ADMOD is consequently located at the center of the anticyclone. Because there is almost no wind at the center of the anticyclone, horizontal advection and divergence of sensible heat flux are negligible. As a result, the only source of air temperature (or input) of ADMOD is δ_R (i.e., the estimated T_A field mostly depends on δ_R, which is constant). This configuration cannot lead to accurate estimates, and a more evolved parameterization needs to be developed in this case. However, this behavior of ADMOD in anticyclonic conditions is not really a weakness of the method given that strong anticyclonic cases may be avoided before ADMOD is applied.

b. ADMOD versus ARPEGE

ADMOD is forced using input variables from 19 low-divergence ARPEGE reanalyses. The T_A and H_s estimates are then compared with corresponding ARPEGE fields, with more than 49 000 points of comparison. Figure 1c shows that ADMOD T_A estimates and ARPEGE T_A match well. The increased resolution in comparison with section 4a analysis does not virtually affect the accuracy of the method. Indeed, the correlation is again high (0.89), the rms deviation is 0.69°C, and the bias is −0.06°C. Note that the bias is negligible, which confirms that the optimal value of δ_R based on the ECMWF analyses is also optimal for ARPEGE. Peak deviations are +5.3° and −1.6°C, which are larger than

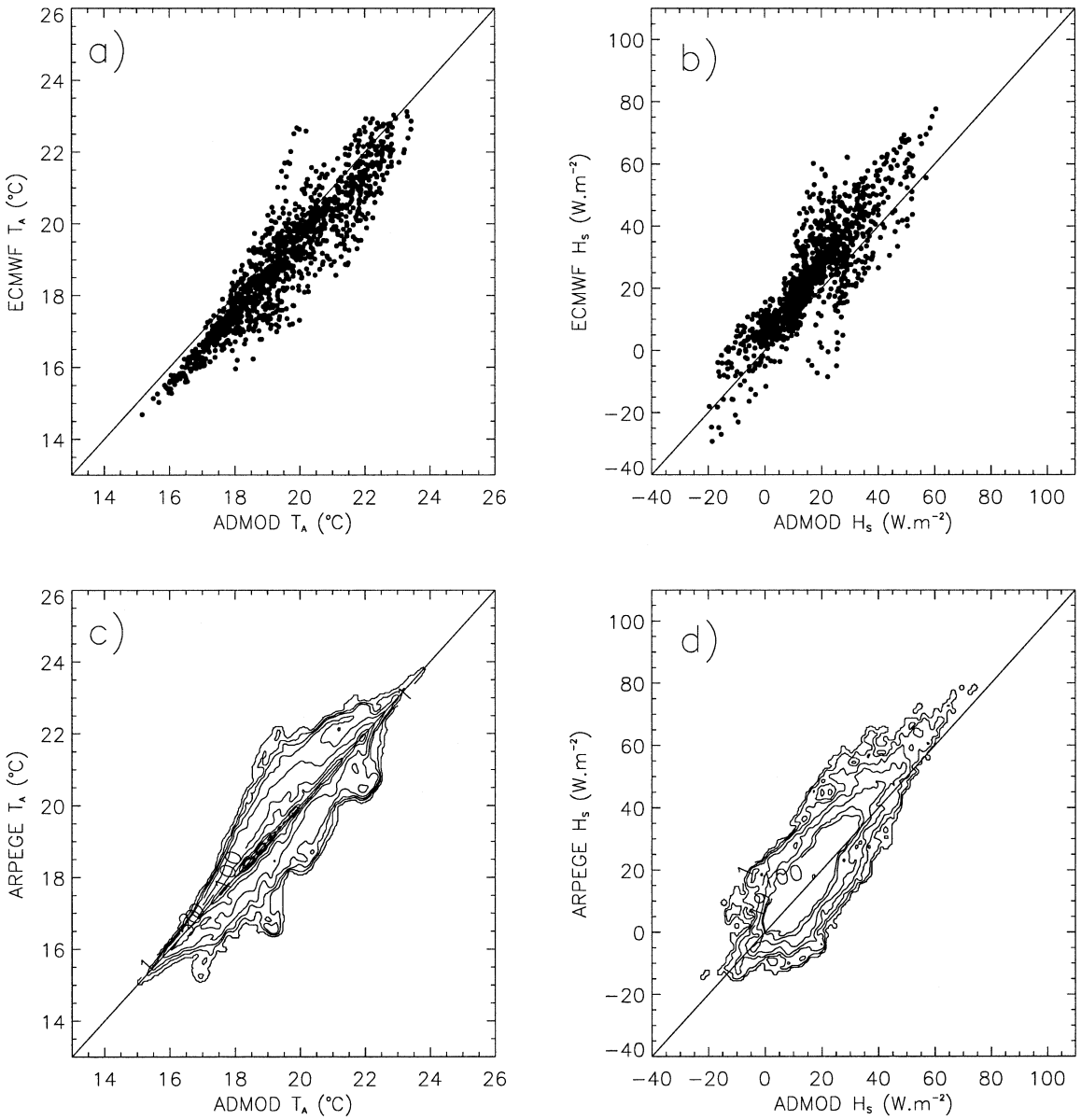

FIG. 1. (a), (b) ADMOD T_A and H_s are compared with ECMWF and with (c), (d) ARPEGE T_A and H_s. In (a) and (b) [(c) and (d)], ECMWF (ARPEGE) fields are used to force ADMOD. Contour lines in (c) and (d) represent the density of points. Units are in number of points per (c) 0.1°C × 0.1°C area and (d) 0.5 W m^{-2} × 0.5 W m^{-2} area.

in section 4a because of the increased spatial resolution of the reanalyses with respect to the analyses. In fact, the analyses have less spatial variability than the reanalyses because of their coarser resolution. The correlation between individual ADMOD and ARPEGE T_A fields is always larger than 0.6 and is greater than 0.8 in 15 of 19 cases. The correlation between ADMOD and ARPEGE fluxes on all data is 0.82, the rms deviation 8.1 W m^{-2}, and the bias −2.6 W m^{-2} (Fig. 1d).

ADMOD, ARPEGE, and ECMWF physics are consistent in terms of T_A and H_s, in most cases. The intrinsic rms error of ADMOD is 0.7°C in T_A and 9 W m^{-2} in H_s, which does not include the error on the input parameters. ADMOD accuracy strongly depends on the quality of T_A at the boundaries, especially close to the inflow boundaries, as detailed in appendix B. According to the sensitivity study reported in appendix B, the fact that h is a constant equal to 580 m has no significant influence on ADMOD estimations in most cases during SEMAPHORE. The sensitivity of ADMOD to h is relatively low, which is of interest in an operational point of view, and the sensitivity to γ_{p_S} is negligible, that is, smaller than 1 W m^{-2} at maximum. In contrast, although the impact of a constant β_{q_A} is negligible if H_s is positive, it may reach 6 W m^{-2} when negative, that is, when warm air is advected over colder water. Although it

happens in only 7% of the cases during SEMAPHORE, it would be interesting to derive β_{q_A} from satellite data in a further study.

5. Application of ADMOD to SEMAPHORE data

In this section ADMOD is run on the input dataset described in section 3a. The estimates of T_A and H_s are successively compared with validation data. First, ADMOD individual retrievals are compared with in situ observations and corresponding ECMWF and ARPEGE data. Next, the ADMOD fields are compared with these GCM fields. For simplicity, ADMOD is named EADMOD (AADMOD) when ECMWF (ARPEGE) T_A are used as boundary conditions.

a. T_A validation

Comparisons between in situ T_A and EADMOD T_A are shown in Fig. 2a. The rms between EADMOD and the R/V is 0.97°C, which is comparable to the intrinsic error of ADMOD (section 4). The correlation coefficient is 0.87, and the bias is −0.18°C (Table 3, line 3). In Fig. 2a, four points corresponding to 19 October are strongly biased for EADMOD and the two GCMs, by 2°C. We consider these points to be erroneous R/V measurements because there is no noticeable discrepancy between the R/V and EADMOD in terms of wind speed or SST for 19 October. If these four points are omitted, the rms error drops to 0.30°C, the correlation becomes 0.99, and the bias is −0.58 (Table 3, line 8). The results reported in Table 3 in lines 6–8 reveal that the R/V data have a better fit to EADMOD than to ECMWF or ARPEGE. Note that the comparisons include so few points that these figures may not be accurate, although the points available already cover a large range of T_A values (almost 7°C). To test how ADMOD behaves with respect to R/V data for another kind of boundary conditions, ARPEGE boundary T_A are used to force ADMOD. The correlation coefficient between AADMOD and R/V T_A is 0.98. The rms error is 0.40°C, which is slightly larger than the EADMOD rms error (0.30°C), and the bias is 0.50°C, which is larger by 1.1°C than the EADMOD bias (Fig. 2b; Table 3, lines 8, 9). This result suggests that the kind of ADMOD boundary conditions used affects mainly the ADMOD estimates as a bias. It also affects the rms error, at a lower level.

To compare T_A from ARPEGE, ECMWF, EADMOD, and AADMOD, all the fields are interpolated at 1.125° × 1.125°, the lowest of the resolutions among these kinds of data. The rms deviation between EADMOD T_A and ECMWF T_A is 0.59°C, and it is 1.06°C between EADMOD and ARPEGE; the biases are 0.30° and −1.00°C, respectively. This result confirms that the use of ECMWF boundary conditions to force ADMOD favors the comparison between EADMOD and ECMWF in terms of bias and rms. The comparison among AADMOD, ARPEGE, and ECMWF fields brings a further

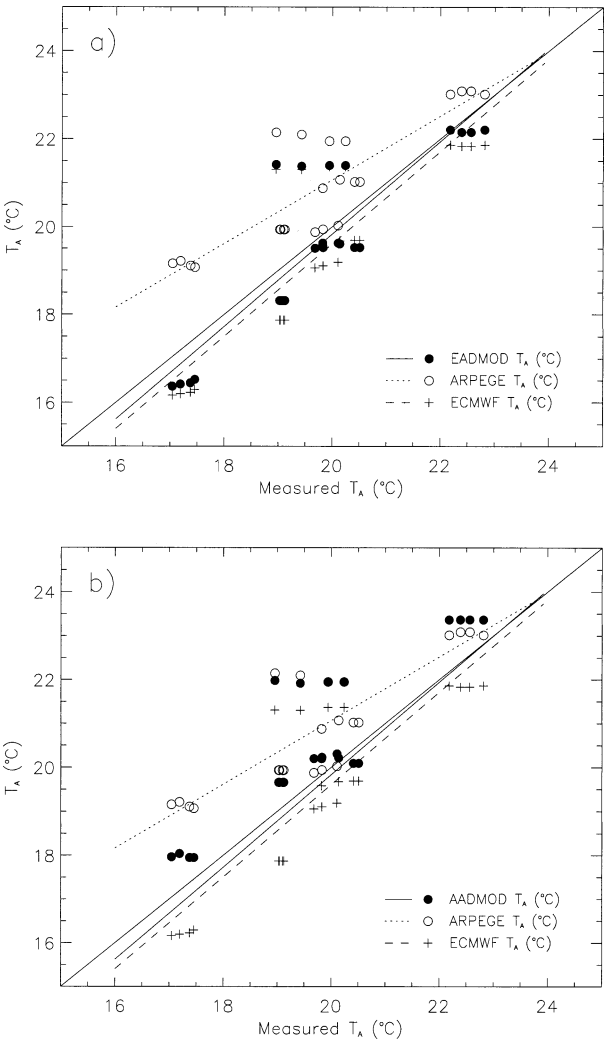

FIG. 2. Validation of (a) EADMOD and (b) AADMOD T_A estimates. The R/V measurements (x axis) are compared with EADMOD/AADMOD (dots), ARPEGE (circles), and ECMWF (crosses) T_A.

confirmation of this result. Indeed, the rms between AADMOD and ARPEGE is smaller by 0.2°C than the rms between ECMWF and AADMOD (Table 4). The results presented in Table 4 show that ADMOD T_A are consistent with T_A from the two GCMs. Note that a perfect agreement among the different models is not to be expected given that ARPEGE, ECMWF, ADMOD are independent, except for the boundary conditions used in ADMOD. Figures 3 and 4 show the case of 0000 UTC 19 October 1993. In Fig. 3i, ADMOD is applied in a typical operational context; that is, ECMWF analyses are used as boundary conditions. In Fig. 4a, ADMOD is applied using ARPEGE boundary conditions. Figures 3g–i and 4a illustrate that, close to the inflow boundaries—that is, south and east of the domain—EADMOD (AADMOD) T_A are very similar to ECMWF (ARPEGE) T_A. In contrast, EADMOD and

TABLE 3. Comparison among R/V, ADMOD, ARPEGE, and ECMWF T_A and H_s. ADMOD inputs are satellite-derived winds and SSTs and ECMWF (or ARPEGE) boundary conditions. Column 3 indicates whether all the points of comparison are used (all) or four points suspected to be erroneous R/V measurements are omitted from the comparisons (corr).

Variable compared	Boundary conditions	Points selected	Kind of data compared	Correlation coef	Rmse (°C)	Bias (°C)
T_A		All	ARPEGE–R/V	0.85	0.85	1.14
—		—	ECMWF–R/V	0.86	1.04	−0.40
—	ECMWF	—	ARPEGE–ECMWF	0.87	0.97	−0.18
—	ARPEGE	—	ARPEGE–R/V	0.89	0.82	0.82
—		—	ECMWF–R/V	0.96	0.79	1.54
—		Corr	ADMOD–R/F	0.95	0.62	0.87
—		—	ECMWF–R/V	0.99	0.31	−0.84
—	ECMWF	—	ADMOD–R/V	0.99	0.30	−0.58
—	ARPEGE	—	ADMOD–R/V	0.98	0.40	0.50
—		—	ARPEGE–ECMWF	0.95	0.76	1.72
H_s		All	ARPEGE–R/V	0.01	11.3	−14.1
—		—	ECMWF–R/V	0.46	13.9	2.2
—	ECMWF	—	ADMOD–R/V	0.15	12.2	−5.9
—	ARPEGE	—	ADMOD–R/V	0.11	11.8	−14.3
—		—	ARPEGE–ECMWF	0.63	12.3	−16.3
—		Corr	ARPEGE–R/V	0.54	6.6	−10.0
—		—	ECMWF–R/V	0.93	8.1	7.3
—	ECMWF	—	ADMOD–R/V	0.79	5.0	−1.1
—	ARPEGE	—	ADMOD–R/V	0.66	6.1	−9.9
—		—	ARPEGE–ECMWF	0.43	13.4	−17.3

AADMOD fields are more consistent far from the inflow boundaries (i.e., north of the domain).

b. H_s validation

In this section, ADMOD fluxes are compared with R/V, ECMWF, and ARPEGE fluxes. Although the ECMWF and ARPEGE already provide H_s flux fields, the bulk algorithm described in section 2 is used to compute new fluxes from these two model SST, T_A, and **u** fields. This computation is intended to minimize the effect of differences among the flux parameterizations used in ADMOD, ARPEGE, and the ECMWF model in the following comparison.

As shown in Fig. 5a, R/V and EADMOD fluxes compare fairly well except for the four underestimated points described previously. They correspond here to positive R/V and negative ECMWF, EADMOD, and ARPEGE fluxes. If these four points are omitted, the correlation coefficient between the R/V and EADMOD H_s is 0.79, the rms deviation is -5.0 W m^{-2}, and the bias is -1.1 W m^{-2} (Table 3, line 18). The bias is small with respect to the biases in ARPEGE and ECMWF H_s (Table 3, lines 16, 17; Figs. 5c,d). The comparison between AADMOD H_s and R/V H_s is shown in Fig. 5b. The correlation coefficient is 0.66, which is smaller than the correlation between EADMOD H_s and R/V H_s (Table 3, line 19).

The rms deviation between EADMOD and ECMWF H_s fields is 9.8 W m^{-2}, and the rms is 12.1 W m^{-2} between EADMOD and ARPEGE (Table 4). On the other hand, the rms deviation between AADMOD and ECMWF H_s fields is 15.4 W m^{-2}, and the rms is 7.0 W m^{-2} between AADMOD and ARPEGE. These results show that the choice of the boundary conditions has a strong impact on the deviations observed between ADMOD and the GCM fields in terms of H_s. The reason is that H_s is sensitive to any change in **u**, T_A, or SST, which are all different in ADMOD, ECMWF, and ARPEGE. The results presented in Table 4 show that the proposed method does not diverge from the two GCMs. In addition, the horizontal variations of H_s of ADMOD

TABLE 4. Comparison among ADMOD, ARPEGE, and ECMWF T_A and H_s fields. ADMOD inputs are satellite-derived winds and SSTs and ECMWF (or ARPEGE) boundary conditions.

Variable compared	Boundary conditions	Kind of data compared	Correlation coef	Rmse (°C)	Bias (°C)
T_A	ECMWF	ADMOD–ECMWF	0.95	0.59	0.30
—	—	ADMOD–ARPEGE	0.83	1.06	−1.00
T_A	ARPEGE	ADMOD–ECMWF	0.90	0.85	1.26
—	—	ADMOD–ARPEGE	0.91	0.65	−0.06
H_s	ECMWF	ADMOD–ECMWF	0.88	9.8	−11.5
—	—	ADMOD–ARPEGE	0.49	12.1	4.22
H_s	ARPEGE	ADMOD–ECMWF	0.62	15.4	−20.5
—	—	ADMOD–ARPEGE	0.67	7.0	−4.8

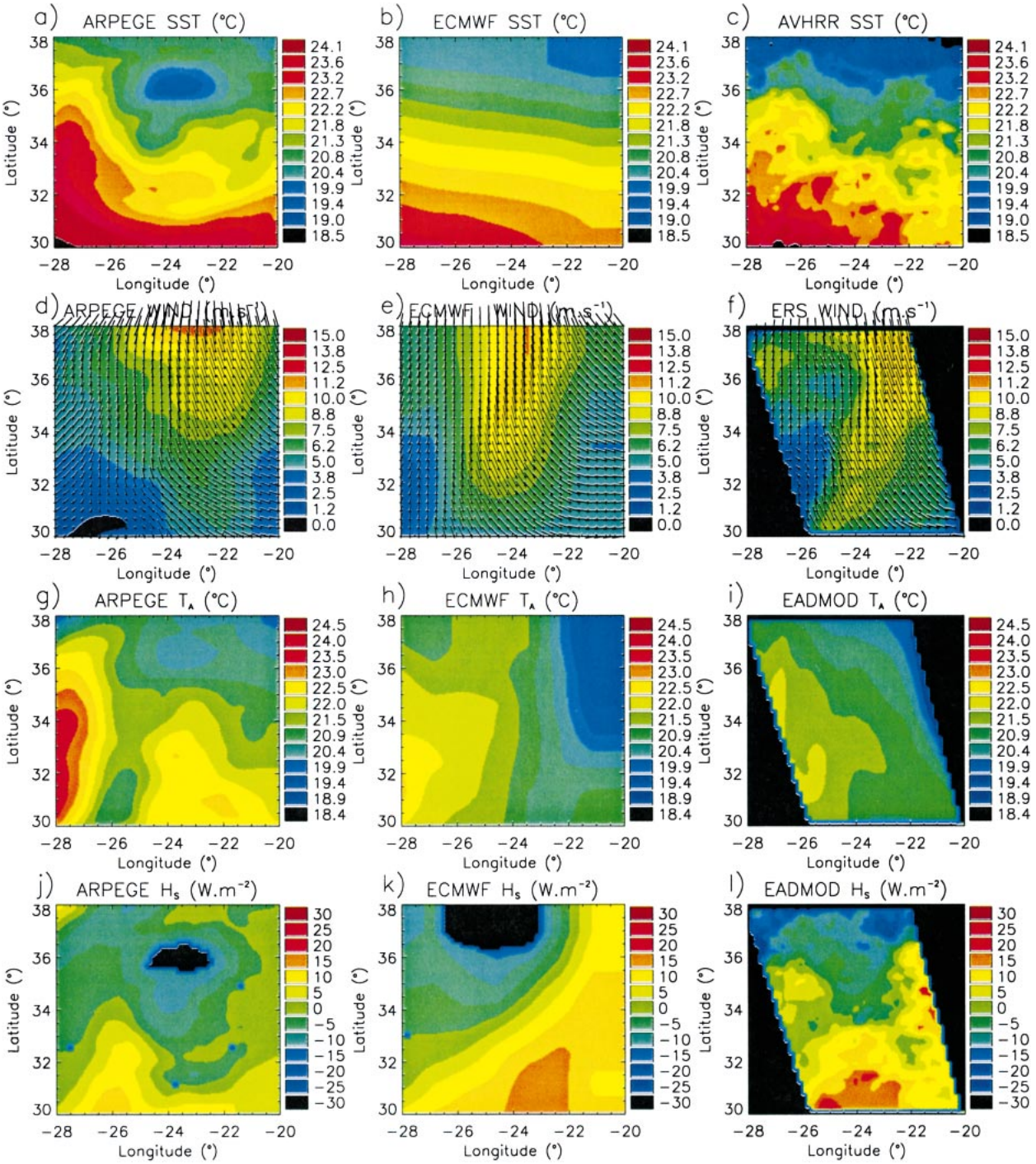

FIG. 3. Comparison among [(a), (d), (g), (j)] ARPEGE, [(b), (e), (h), (k)] ECMWF, and [(i), (l)] ADMOD fields on 0000 UTC 19 Oct 1993. The fields used to force ADMOD are (c) AVHRR SSTs, *ERS-1* wind vectors, and (h) ECMWF T_A around the SEMAPHORE region.

and the GCMs are consistent for the six cases of the dataset: the ADMOD flux fields observed one by one often possess the same flux structures as in the ECMWF model and ARPEGE, but they are deformed in accordance to *ERS-1* wind field and AVHRR SSTs. Plus, EADMOD fluxes always reveal high-resolution details. The case of 0000 UTC 19 October presented in Figs. 3j–l and 4b illustrates that EADMOD (AADMOD) refines the H_s ECMWF (ARPEGE) structures. A large structure of strong fluxes is present southeast of the SEMAPHORE zone in the ECMWF H_s analysis, whereas EADMOD simulates a more detailed structure. Note

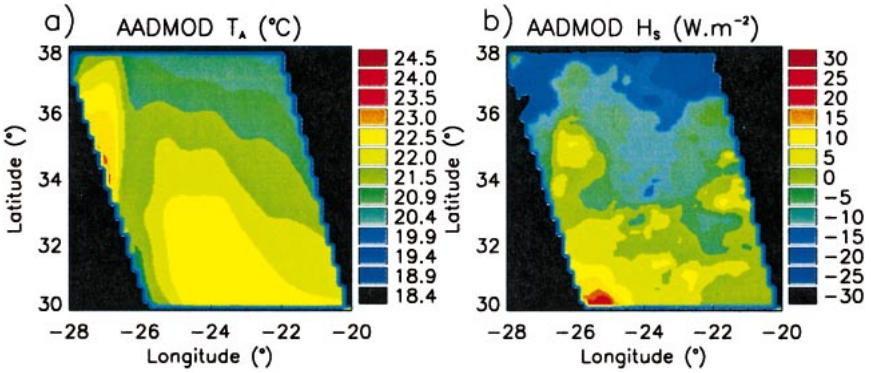

FIG. 4. ADMOD (a) T_A and (b) H_s fields on 0000 UTC 19 Oct 1993. The fields used to force ADMOD are AVHRR SSTs, *ERS-1* wind vectors, and ARPEGE T_A around the SEMAPHORE region.

that EADMOD and AADMOD feature remarkably similar H_s fields, given that they use different boundary conditions (Figs. 3l and 4b). In particular, a spot of large H_s can be noticed at 35°N, 26°W in Figs. 3l and 4b. This spot, which is related to high AVHRR SSTs in this area, is not present in the ARPEGE or ECMWF fields (Figs. 3j,k).

6. Conclusions

An original method to derive mesoscale sensible heat flux fields from satellite data, in situ measurements, and GCM operational analyses was proposed. The method is based on a horizontal advection temperature model. In the context of a field experiment, GCM operational

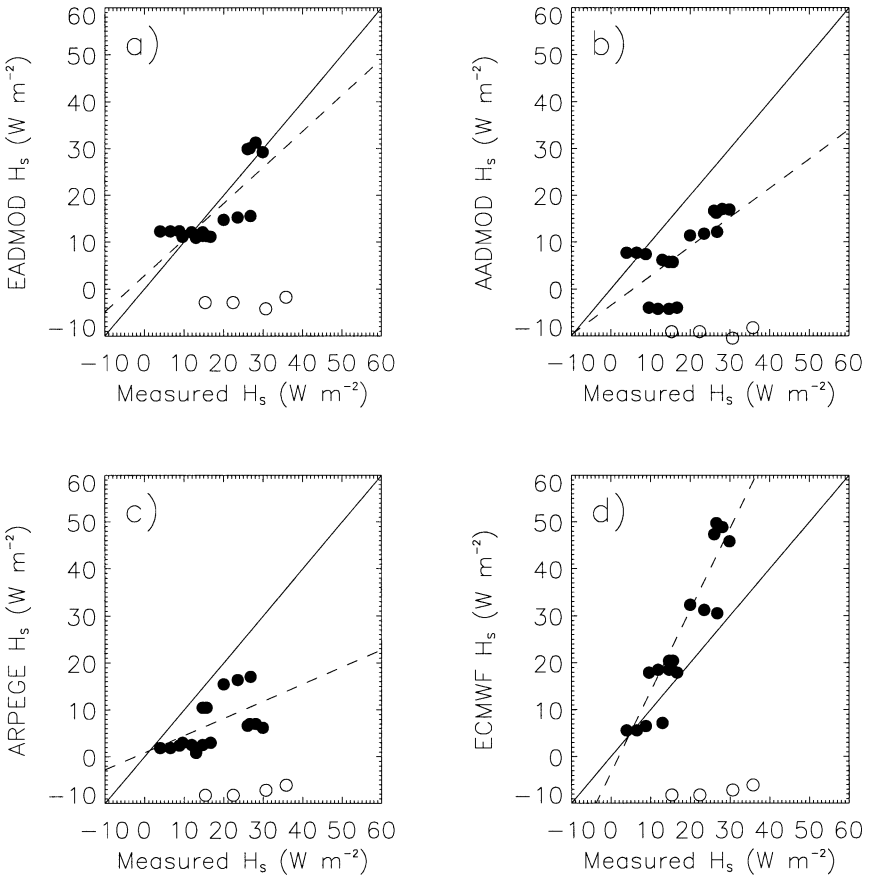

FIG. 5. Validation of ADMOD H_s estimates. The R/V measurements are compared with (a) EADMOD and (b) AADMOD fluxes. The R/V fluxes are compared with (c) ARPEGE fluxes and (d) ECMWF fluxes.

analyses are often the only available source to obtain T_A and H_s fields. The method proposed may help to enhance these fields in resolution and accuracy. Plus, the method is computationally fast to run, as opposed to the intensive process that consists of assimilating satellite data in GCMs. Although the physics involved in the method proposed is simple, it was found to be consistent with two GCMs during 1 month from 15 October to 15 November 1993, in a near-subtropical zone of the North Atlantic. The intrinsic error of the method is 0.7°C for T_A and 9 W m^{-2} for H_s, both at 1.125° × 1.125° and 0.16° × 0.16° resolution. The main weaknesses of the method are a larger retrieval error, by 6 W m^{-2} in rms when H_s is negative, and the fact it is unable to treat cases of strong atmospheric front because the flow is assumed to be steady.

The method was applied to *ERS-1* wind vectors, AVHRR SSTs, and either ECMWF or ARPEGE T_A conditions. The comparison between the T_A and H_s retrievals and R/V data gave the following rms errors: 0.3°C and 5 W m^{-2}, which is encouraging because these errors are smaller than the estimated intrinsic error of the method. The kind of boundary conditions used in ADMOD mainly affects the bias. It also affects the rms error at a lower level. Although too few points of comparisons are available to consider these results to be final, they may be compared with Jones et al. (1999) error, 0.72° ± 0.38°C, which was obtained from data averaged over 1 month. For H_s, if we consider the following errors in the input parameters: 1 m s^{-1} for **u**, 0.5°C for SST, and 0.5°C for T_A, the accuracy of the method proposed is in the range of 15–20 W m^{-2}, which is smaller than the error found by Konda and Imasato (1996) by 17 W m^{-2}. Note that these comparisons may not be accurate because the Jones et al. (1999) and Konda and Imasato (1996) studies are based on several years of data, with air temperatures ranging from ~2° to ~32°C, whereas the SEMAPHORE data cover only 1 month, with air temperatures in the range of 15°–23°C.

Acknowledgments. This study was performed, in part at JPL, California Institute of Technology, under contract with the National Aeronautics and Space Administration (NASA). It was partly supported by the Physical Oceanography Program of NASA. This work was also performed under contract with French Direction Générale de l'armement, Direction de la Recherche et de la Technologie (DGA-DRET), and Centre National de la Recherche Scientifique (CNRS). The authors acknowledge the JPL PODAAC; IFREMER; the ECMWF; the Centre de Meteorologie Spatiale (CMS) of Météo France; H. Giordani from Météo France, who provided the ARPEGE reanalyses; and I.-Lin Tang. The authors are grateful to Dr. A. Bingham and the *Journal of Applied Meteorology* reviewers; their comments allowed us to improve the model presented in this paper.

APPENDIX A

Numerical Solution

First-order finite differences and a relaxation method are used to solve the model numerically. The relaxation method consists of adding $\partial\theta/\partial t$ to (3) and running the model until convergence is achieved. The advection terms are discretized using an upwind difference scheme to avoid numerical instabilities. The time step Δt is local to accelerate convergence. Its expression is

$$\Delta t_{i,j} = 0.85\frac{\delta x}{U_{i,j}}, \tag{A1}$$

where i, j are the gridpoint coordinates on the discrete domain; δx is the spatial step; and $U_{i,j}$ is the horizontal scalar wind at i, j. At each time step, the temperature is updated at grid points for which wind speed data are available. This technique is useful because sparse satellite input fields are used to force ADMOD, that is, fields that contain gaps. Convergence is stopped when the residual of all temperature updates between time steps n and $n + 1$ is smaller than 0.001°C, which usually happens after 80–100 iterations. The process lasts about 30 s on a standard workstation, for a 50 × 50 gridpoint domain.

APPENDIX B

Sensitivity Study

In this section, the sensitivity of ADMOD to error in the boundary conditions and in h, β_{q_A}, and γ_{p_S} is studied.

a. Sensitivity to the boundary conditions

The sensitivity of the T_A retrieval error to the error on T_A at the boundaries is studied as a function of h.

An analytical solution of ADMOD is obtained in the one-dimensional case, assuming that there is no vertical

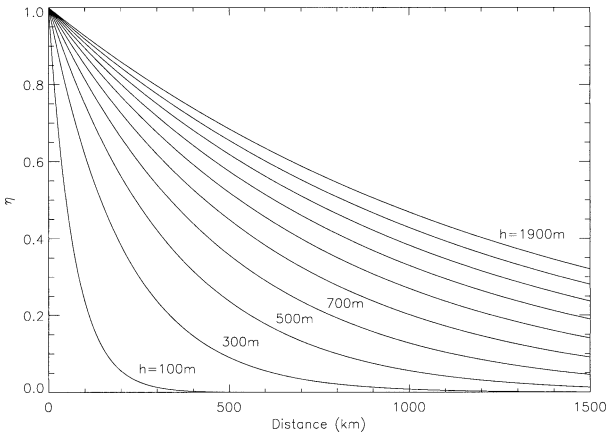

FIG. B1. Sensitivity curves for η showing the impact of an error in T_A at the boundary on the error in T_A inside the region under study. Sensitivity is studied as a function of the distance from the boundary.

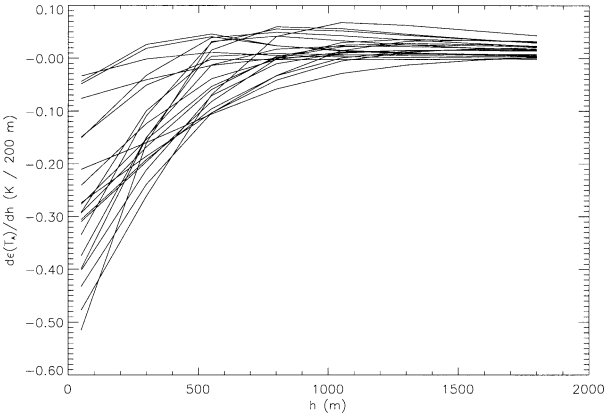

FIG. B2. Sensitivity of ADMOD T_A to a change in h. Each curve corresponds to a particular date among 20 cases. The y axis represents the derivative of the rms deviation between ADMOD and ARPEGE T_A fields with respect to h.

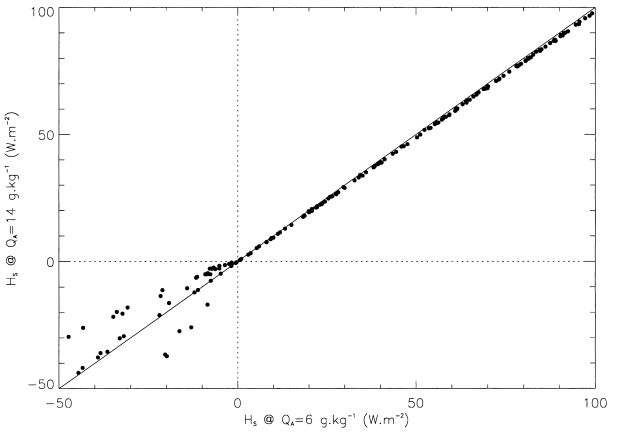

FIG. B4. Sensitivity of the bulk fluxes to β_{q_A}. On a synthetic dataset that represents the SST, T_A, wind, and pressure conditions observed during SEMAPHORE, flux values are computed using $\beta_{q_A} = 6$ and 14 g kg^{-1}, respectively, which are extrema during SEMAPHORE.

wind speed, no SST gradient, and that **u** is positive. In addition, f is replaced with a bulk formula using a constant C_H of 1.2×10^{-3} in (3). The solution is

$$T(x) = T(0) \exp\left(\frac{\alpha}{h} C_H x\right) + \text{SST}, \tag{B1}$$

where x is the distance from the inflow boundary, $T(0)$ is the boundary condition, and $T(x)$ is the estimated temperature at x. The errors $\epsilon_{T(0)}$ and $\epsilon_{T(x)}$ in $T(0)$ and $T(x)$ are defined as

$$\epsilon_{T(0)} = T(0)_{\text{true}} - T(0)_{\text{err}} \quad \text{and} \tag{B2}$$

$$\epsilon_{T(x)} = T(x)_{\text{true}} - T(x)_{\text{err}}, \tag{B3}$$

where T_{err} is the air temperature that includes error ϵ. Next, the ratio η between the two errors $\epsilon_{T(0)}$ and $\epsilon_{T(x)}$ is defined [(B4)] to study the impact of an error at the boundary on the error at x:

$$\eta = \epsilon_{T(x)} / \epsilon_{T(0)}. \tag{B4}$$

Last, (B1)–(B4) are combined to obtain the sensitivity curves shown in Fig. B1. They point out that η depends strongly on h, and the error in T_A virtually does not depend on the error in the boundary conditions as h tends toward low numbers. At $h = 580$ m, which is the value used throughout this paper, the error in $T(0)$ is decreased by 50% in 300 km. For an 800 km $\times$ 800 km region, it means that the half of the region that is the closest to the inflow boundaries will be strongly affected by an error at the boundaries ($\eta > 50\%$), whereas the other half-region will be less affected. A more accurate estimation of the sensitivity to the boundary errors would require a case-by-case analysis because the maximum distance of a point from the inflow boundaries may vary from 50 to 1100 km, depending on the curvature of the streamlines. However, only low-divergence

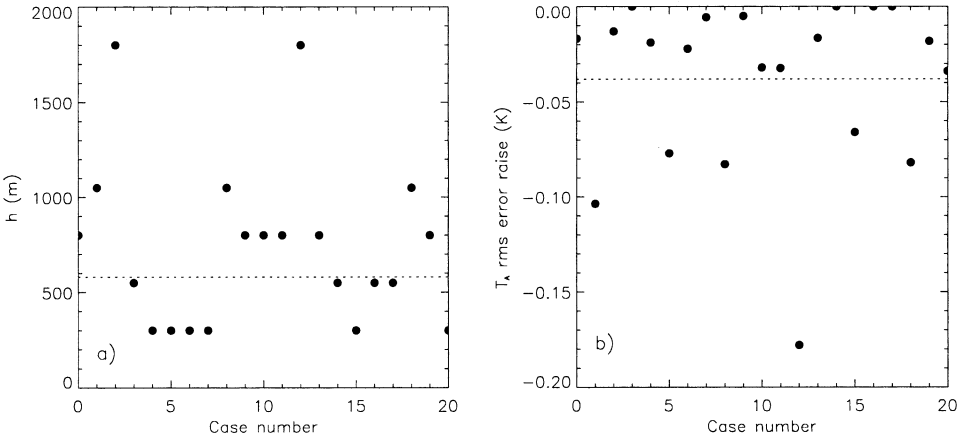

FIG. B3. (left) The dots represent the optimal h derived for 20 cases. The dotted line is the constant $h = 580$ m used throughout the paper. (right) The increase in T_A rms error due to the use of $h = 580$ m instead of the optimal h.

cases are considered in this paper, so the curvature of the streamlines is small (see Figs. 3d–f, for instance). As a result, the explanation above generally applies to SEMAPHORE. Note that, in the full ADMOD, η depends also on **u** in a way such that η is lower as **u** increases. The error in T_A at the boundaries eventually may have a strong impact on the quality of the results, especially at high h numbers, so that it is recommended to use boundary conditions that are as accurate as possible.

b. Sensitivity to h

Twenty-one low-divergence ARPEGE reanalyses from the test dataset (section 3c) and an h that varies from 50 to 1800 m by increments of 250 m, instead of being a 580-m constant, are used to force ADMOD. Then, the rms deviation between ARPEGE and ADMOD T_A is studied as a function of h. As shown in Fig. B2, a change in h by 200 m around $h = 580$ m modifies the rms deviation by 0.15°C, which is low. However, the sensitivity to h increases up to 0.5°C $(200\ \text{m})^{-1}$ as h tends toward 0.

For each of the 21 cases, an optimal h is derived as the minimum T_A rms deviation between ADMOD and ARPEGE observed while h ranges from 50 to 1800 m. The average of these optimal h is 740 m, which is not far from 580 m. The optimal h may be very different from 580 m in individual cases, by 1200 m at maximum (Fig. B3a), but the rms deviation loss corresponding to the use of $h = 580$ m in ADMOD instead of the optimal h is never larger than 0.2°C (Fig. B3b). The reason is that most of the optimal h are greater than 600 m, beyond which the sensitivity of the model to h is lower.

c. Sensitivity to β_{q_A} and γ_{p_S}

To check if the assumption of a constant β_{q_A} is not too strong, two sets of 550 runs of the bulk flux algorithm f (section 2) are performed using, respectively, $\beta_{q_A} = 6\ \text{g kg}^{-1}$ and $\beta_{q_A} = 14\ \text{g kg}^{-1}$, which are the extrema during SEMAPHORE. The other flux parameters **u**, T_A, γ_{p_S}, and SST are randomly selected within the range of maximum and minimum values observed during SEMAPHORE. As shown in Fig. B4, the comparison between the sensible heat fluxes at 6 and 14 g kg^{-1} is negligible for the positive fluxes, the rms deviation being 0.4 W m^{-2}. However, the rms error becomes 6 W m^{-2} for the negative fluxes.

A similar technique is used to find that the sensitivity to γ_{p_S} is negligible: for fluxes ranging from -50 to 150 W m^{-2} the rms deviation between H_s obtained at 990 and 1040 hPa is lower than 1 W m^{-2}. Only 2 of 548 points of comparison are biased and correspond again to negative H_s.

REFERENCES

Bourassa, M. A., M. H. Freilich, D. M. Legler, W. T. Liu, and J. J. O'Brien, 1997: Wind observations from new satellite and research vessels agree. *EOS Trans. Amer. Geophys. Union,* **78,** 597–602.

Bourras, D., 2000: Calcul des flux turbulents au dessus des océans par la méthode bulk. (Calculation of turbulent fluxes over oceans using the bulk method.) Centre d'Etude des Environnements Terrestre et Planétaires Tech. Note RI-CETP/2/2000 54 pp. [Available from CETP, 10–12 av. de l'Europe, 78140, Vélizy, France.]

——, L. Eymard, and W. T. Liu, 2001: A neural network to estimate the latent heat flux over oceans from satellite observations. *Int. J. Remote Sens.*, in press.

Caniaux, G., and S. Planton, 1998: A three-dimensional ocean mesoscale simulation using data from the SEMAPHORE experiment: Mixed layer heat budget. *J. Geophys. Res.*, **103,** 25 081–25 099.

Clayson, C. A., and J. A. Curry, 1996: Determination of surface turbulent fluxes for the Tropical Ocean Global Atmosphere Coupled Ocean–Atmosphere Response Experiment: Comparison of satellite retrievals and in situ measurements. *J. Geophys. Res.*, **101,** 28 515–28 528.

Dupuis, H., P. K. Taylor, and A. Weill, 1997: Inertial dissipation method applied to derive turbulent fluxes over the ocean during the Surface of the Ocean, Fluxes and Interactions with the Atmosphere/Atlantic Stratocumulus Transition Experiment (SOFIA/ASTEX) and Structure des Echanges Mer–Atmosphere, Proprietes des Heterogeneites Oceaniques: Recherche Experimentale (SEMAPHORE) experiments with low to moderate wind speed. *J. Geophys. Res.*, **102,** 21 115–21 129.

Eymard, L., and Coauthors, 1996: Study of the air–sea interactions at the mesoscale: The SEMAPHORE experiment. *Ann. Geophys.*, **14,** 986–1015.

Giordani, H., S. Planton, B. Bénech, and B. H. Kwon, 1998: Atmospheric boundary layer response to sea surface temperatures during the SEMAPHORE experiment. *J. Geophys. Res.*, **103,** 25 047–25 060.

Jones, C., P. Peterson, and C. Gautier, 1999: A new satellite method for deriving ocean surface specific humidity and air temperature: An artificial neural network approach. *J. Appl. Meteor.*, **38,** 1229–1245.

Kilpatrick, A., G. P. Podesta, and R. Evans, 2001: Overview of the NOAA/NASA Advanced Very-High Resolution Radiometer Pathfinder algorithm for sea surface temperature and associated matchup database. *J. Geophys. Res.*, **106,** 9179–9197.

Konda, M., and N. Imasato, 1996: A new method to determine near-sea surface air temperature by using satellite data. *J. Geophys. Res.*, **101,** 14 349–14 360.

Kwon, B. H., B. Bénech, D. Lambert, P. Durand, A. Druilhet, H. Giordani, and S. Planton, 1998: Structure of the marine atmospheric boundary layer over an oceanic thermal front: SEMAPHORE experiment. *J. Geophys. Res.*, **103,** 25 159–25 180.

Lambert, D., and P. Durand, 1999: The marine atmospheric boundary layer during SEMAPHORE. I: Mean vertical structure and nonaxisymmetry of turbulence. *Quart. J. Roy. Meteor.*, **125,** 495–512.

Liu, W. T., and P. P. Niiler, 1984: Determination of monthly mean humidity in the atmospheric surface layer over oceans from satellite data. *J. Phys. Oceanogr.*, **14,** 1451–1457.

Seager, R., M. B. Blumenthal, and Y. Kushnir, 1995: An advective atmospheric mixed layer model for ocean modeling purposes: Global simulation of surface heat fluxes. *J. Climate*, **8,** 1951–1964.

Tennekes, H., 1973: The logarithmic wind profile. *J. Atmos. Sci.*, **30,** 234–238.